Interface Engineering of Graphene /Copper Matrix Composites Decorated with Tungsten Carbide for Enhanced Physico-Mechanical Properties

L.L. Dong [a], Y.Q. Fu [b], Y. Liu [a], J.W. Lu [a], W. Zhang [a], W.T. Huo [a],

L.H. Jin [a], Y.S. Zhang [a, c] *

[a] Advanced Materials Research Central, Northwest Institute for Nonferrous Metal Research, Xi'an 710016, PR China

[b] Faculty of Engineering and Environment, Northumbria University, Newcastle upon Tyne NE1 8ST, UK

[c] Xi'an Rare Metal Materials Institute Co., Ltd, Xi'an, 710016, PR China

ABSTRACT:

For metal matrix composites (MMCs), introduction of low-dimensional nano-carbon materials (NCMs) into three dimensional metallic matrix is commonly applied to enhance mechanical and physical properties of metals and thus significantly extend their wide range applications. However, the interfaces between the NCMs and metal matrix are always a major issue for achieving the best enhancement effects. In this paper, we investigated interfacial structures of graphene nanoplates (GNPs) reinforced Cu matrix composites fabricated using a simple and industrially scalable strategy, through integration of interface engineering design

* Corresponding author:
E-mail: y.sh.zhang@163.com, y.sh.zhang@c-nin.com (Y.S. Zhang)

methodology and a spark plasma sintering process. We then systematically evaluated their physico-mechanical properties, interfacial characteristics and strengthening mechanisms. The *in-situ* formed W_xC_y nano-layers and carbide nanoparticles on the surfaces of GNPs and near the interfaces of Cu grains promote strong interfacial bonding and improves the cohesive strength of Cu based nanocomposites. The GNPs-W/Cu composites show a good balance between strength and electrical conductivity. Their 0.2% yield strength and ultimate tensile strength have been improved up to 239.13% (112.73%) and 197.76% (72.51%), respectively, when compared with those of pure copper (or GNPs/Cu composites). Electrical conductivity of GNPs-W/Cu composites showed no apparent changes after the addition of the GNPs. The dislocation strengthening, refinement strengthening and load transfer strengthening were achieved simultaneously through the engineered interfaces in GNPs-W/Cu matrix composites. This work has provided a new strategy to fabricate high-performance NCMs enhanced MMCs by using the interface engineering methodology.

KEYWORDS: Graphene nanoplates; Interface engineering; Physico-mechanical properties; Cu matrix composites

1. INTRODUCTION

Copper matrix composites (CuMCs) reinforced with nanocarbon materials, including carbon nanotubes (CNTs), graphene and its derivatives (graphene oxide,

graphene nanoplate or GNP, graphene nanoribbon etc.), and carbon fibers, are important structural and functional composites materials which possess good thermal/electrical conductivities, mechanical properties and wear resistance. They have found many applications in the fields of electrodes, rail transportation, electronic packaging and electrical contacts [1-3].

Various fabrication techniques, including hot pressing sintering, spark plasma sintering (SPS), microwave sintering, etc. have been developed in the past many years to produce the CuMCs using graphene as a reinforcement owing to its unique structure and extraordinary physical/mechanical properties [4-8]. For example, Hu et al. fabricated graphene reinforced Cu nanocomposites using a laser sintering method and achieved a 22% increase in Vickers hardness [9]. Shao et al. [10] prepared graphene nanoplates/copper (GNPs/Cu) matrix composites using electrostatic self-assembly and SPS, and found that 0.2 wt% addition of GNPs into Cu matrix resulted in a 27% increase of the tensile strength up to 233 MPa and a 19% increase of hardness up to 108.6 HV. C. Ayyappadas et al. [11] studied effect of combined microwave and conventionally sintered processes on physical properties of graphene/Cu composites, and reported that the densities of microwave sintered samples (89%) were higher than those of the conventional sintered counterparts (86%), and the highest electrical conductivity of the composites was 94 %IACS when the 0.9 vol.% graphene was added. According to literature, when the graphene addition is above ~ 0.6 vol.% [12-14], the mechanical properties of graphene/Cu composites become significantly degraded, which is mainly due to the poor interfacial

bonding structures formed between Cu matrix and graphene, and the poor wettability of carbon materials (e.g., graphene, CNTs, graphite etc.) with metal Cu (e.g., the contact angle between Cu and graphite is 140^{o}) [15].

For nanocomposites, an excellent interfacial bonding is the key to ensure the remarkable mechanical and physical properties. Many publications have reported that graphene and metals (especially Cu, Mg and Ni matrixes) are mechanically bonded, but not chemically bonded, thus resulting in inferior mechanical properties of the composites [11, 16]. However, carbon materials coated with a suitable metal layer of Ni or Cu [17, 18] were reported to have improved interfacial adhesion between carbon and metal matrix owing to the good chemical affinity of the metal to both carbon and metal matrix [19]. We previously introduced Cu-coated graphene nanoplates (Cu@GNPs) into the copper tungsten composites using electroless plating and spark plasma infiltrating sintering [17]. Results showed that an electrical conductivity of 38.512 M·S/m, a thermal conductivity of 264 $W \cdot m^{-1} \bullet K^{-1}$ and a micro-hardness of 278 HV have been achieved for the sintered copper tungsten composites added with only 0.8 wt.% Cu@GNPs nanopowders, which showed increments of ~95.3%, ~24.3%, and ~28%, respectively, compared with those from the conventionally sintered un-doped copper tungsten powder [17]. Recently, Zhang's group has fabricated Ni@GNPs/Ti composites and achieved a strength of 793 MPa, which is ~40% higher than that of monolithic pure Ti matrix [20].

On the other hand, it has been demonstrated that *in-situ* formed Al_4C_3 at the interfaces between CNTs and Al during the sintering process can significantly

promote the interface adhesion and achieve the effective load transfer of CNTs/Al matrix composites [21]. Similar phenomena have been reported in the GNPs reinforced titanium matrix composites [22, 23]. However, it is impossible for carbon/Cu composites to form interfacial carbides such as those commonly observed in CNTs reinforced Al matrix composites or GNPs reinforced Ti matrix composites, because carbon is not easily chemically reacted with Cu during sintering. Nevertheless, this problem could be easily solved using micro-alloying of Cu matrix through an interface engineering design. Although several sophisticated coating methods have been applied to strengthen the CuMCs so far [12, 14, 18, 19], the enhancement of interfacial bonding has not been found as effective as expected. Thus, the main aim of this work is to apply interface engineering and structural designs, as well as an SPS *in-situ* reaction process to improve the wettability and interfacial bonding between the GNPs and Cu matrix in order to fabricate high performance CuMCs. We purposely introduce *in-situ* formed W_xC_y nano-layers and nanoparticles on the surface of GNPs and near the interfaces of Cu grains to promote strong interfacial bonding and improves the cohesive strength of the Cu based nanocomposites (**Figure 1**), which show a good balance between strength and electrical conductivity. The dislocation strengthening, grain refinement strengthening and load transfer strengthening were simultaneously achieved through the engineered interfaces in GNPs-W/Cu matrix composites. Their interfacial structures, physico-mechanical properties and strengthening mechanism are systematically investigated.

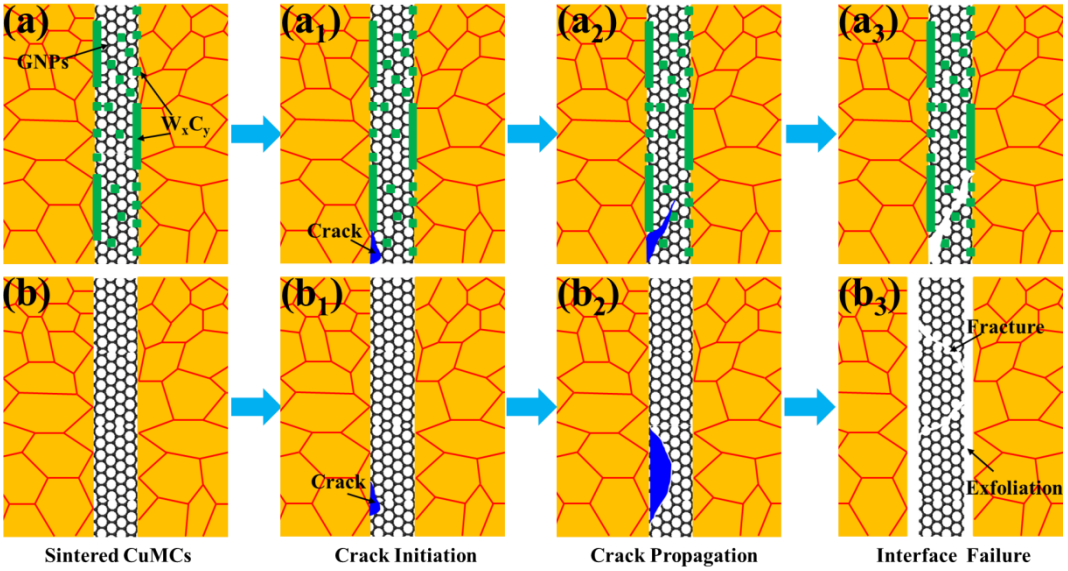

Figure 1. Illustrations of designed interfacial microarchitectures of (a) GNPs-W/Cu matrix composites and GNPs/Cu matrix composites of (b), respectively. (a) shows the W_xC_y nanolayer or nanoparticles formed at the interface of GNPs/Cu or on the surface of GNPs, (a_1) reveals the crack produced at the GNPs/Cu interface under the applied tensile load, (a_2) indicates that the crack propagates along the GNPs/GNPs; and (a_3) shows that interface of W_xC_y/Cu has a good load-transfer capacity. (b) shows the GNPs bond with Cu interface, (b_1) reveals the crack produced at the GNPs/Cu interface under the applied tensile load, (b_2) indicates that the crack propagates along the GNPs/GNPs and GNPs/Cu interface, (b_3) reveals that the fracture of GNPs and GNPs exfoliation at GNPs/Cu interface result in failure of GNPs/Cu composites, respectively.

2. EXPERIMENTAL SECTION

2.1 Source Materials

The average particle sizes of electrolytically processed Cu powders and

commercially available W powders (both obtained from Xing Rong Yuan Technology Co., Ltd., Beijing, China) are 48 μm and 5 ~ 7 μm, respectively. The typical images obtained using a scanning electron microscope (SEM, JEOL JSM-6700F) are shown in **Figures S1a** and **S1b**. Graphene nanoplates (GNPs, 1~3 μm in length and 1~5 nm in thickness) were purchased from XFNANO Materials CO., Ltd., Jiangsu, China, and a typical morphology obtained from a transmission electron microscope (TEM, JEM-3100) is shown in **Figure S1c**. The inverse fast Fourier transform **(**IFFT, inset) image taken at the marked region of **Figure S1c1** shows that the lattice inter-planer spacing is ~ 0.337 nm (**Figure S1c2**), matching with the lattice of (0002) C plane of XXX.

2.2 Preparation of GNPs-W/Cu Matrix Composites

The synthesis method of Cu matrix composites (**Figure S1f**) is summarized as follows: (1) 1 g of GNP powders with the activation agent (3-(N, N-Dimethylmyristylammonio) were added into ethyl alcohol and ultrasonically agitated for about 30 min until they became a homogeneous black solution, indicating that the GNPs were uniformly dispersed into ethyl alcohol; (2) 198 g of pure Cu powders and 1.0 g of W powders were added into the above GNPs solution, and then continuously stirred for 30 min in order to obtain a mixture slurry; (3) The obtained mixture was put into a stainless steel balling jar and then processed with planetary ball milling (QM-3SP2, Nanjing Nan Da Instrument Plant, Jiangsu, China) using stainless steel balls of 2 mm, 5 mm and 8 mm in diameters as milling media, respectively (Mass Ratio, 1:2:3) with a speed of 300 r/min for 5 hrs in an Ar protective atmosphere.

The ball-to-powder weight ratio was 3:1; (4) The ball milled mixed powders were completely dried using a vacuum oven at a temperature of 60 ^{o}C for 24 hrs. An SEM image of as-received GNPs/Cu powders decorated with W powders mixture is shown in **Figure S1d**, which is named as GNPs-W/Cu for simplicity. The flower-like flocculent Cu particles (**Figure S1a**) were crashed into thick flakes (**Figure S1d**), which are in favor of absorption of GNPs and W particles on the Cu powders surface [24, 25]. The GNP clusters are observed on the surface of flaked Cu (marked in **Figure S1d**), in which the enlarged view reveals the winkled morphology (inset, **Figure S1d**). Combined mapping images obtained from energy dispersive X-ray spectroscope (EDS) are shown in **Figure S1e**, in which the W particles and GNPs are uniformly dispersed on the surface of Cu flakes (marked region A in **Figure S1d**). Furthermore, microstructures of the GNPs-W/Cu mixture powders were characterized using the TEM and further investigated by Fast Fourier transform (FFT) and IFFT, and the results are shown in **Figure S2**. Thermal gravimetric analysis (TGA) has been performed in an atmospheric environment to assess (a) material retention after the composite formation and (b) its stability at high temperature. **Figure S3a** shows the TGA curve for GNPs where a major weight loss is observed at 550 ^{o}C, which is related to the thermal decomposition of sp^2 hybridized carbon [26]. **Figure S3b** shows the TGA results of the GNPs/Cu and GNPs-W/Cu mixtures. Results show that during the heating-up process, Cu powders were gradually oxidized into copper oxides. The composite powders were then compacted and densified using an SPS system (SPS-80T) operated at 700 ^{o}C~980 ^{o}C for 20 min under a pressure of 45 MPa.

2.3 Microstructure and Structure Characterization

Chemical element contents in the composite powders and SPS processed composites were measured using an X-Ray fluorescence spectrometer (XRF, Bruker S8 Tiger), and the results are shown in **Figure S4**. The main elements include Cu and W (~0.5 wt%), whereas the other elements (such as Fe, Ba, Cr, etc.) come from the impurities during the measurement test [27]. The GNPs in the composites were characterized using a Raman spectroscope (Micro Raman LabRAM VIS-633) with a He-Ne laser light (532 nm) over the range of 1000 ~ 3000 cm^{-1}. X-ray diffractometer (XRD, Bruker D8 ADVANCE) with Cu-K_α radiation was used to investigate the crystalline structures of the samples. Microstructural evolution, sintering behavior and interfacial structures of the Cu matrix composites were investigated using both the SEM and TEM.

Densities of the SPS processed composites were measured using the Archimedes' method [28], and the theoretical densities were calculated according to that reported in reference [3]. Electrical conductivity measurements were performed using an eddy current method with the D60K digital conductivity meter (Xiamen Xin Bo Technology Co., Ltd, Xiamen, China). Tensile tests were carried out at room temperature using an MTS810 universal testing machine with a strain rate of 1 mm/min. The samples were machined into the dog-bone shaped specimens with a gauge width of 4 mm and a gauge length of 16 mm. At least three measurements were performed for each parameter in order to acquire an average value. The fracture

surface morphologies and its surface compositions after the tensile tests were characterized using the SEM equipped with an EDS.

In order to study the micro- and nanoscale fracture behavior of the GNPs-W/Cu composites, *in-situ* tensile tests were further performed using a miniaturized deformation device within the SEM. The microscale tensile sample was machined from as-sintered composites into a flat dumbbell shape, which had a gauge length of 6 mm and a cross-section of 2 mm × 0.8 mm. A tiny notch (with a depth of 0.02 mm) was pre-made using wire-electrode cutting on the side of the samples to prepare the fracture position. The prepared microscale sample was further mechanically and electrochemically polished. During the entire tensile tests, the process was paused several times in order to observe the fracture process in real time using the SEM.

3. RESULTS AND DISCUSSION

3.1 MICROSTRUCTURE AND CRYSTALLINE STRUCTURE

The typical TEM images of GNPs-W/Cu composites are presented in **Figure 2**. It can be seen in **Figure 2a** that GNPs with a width of ~ 500 nm are well embedded and bonded with the Cu matrix without the presence of cracks. Furthermore, a few *in-situ* formed nanoparticles with sizes of 15~20 nm (point A) appear within the GNPs and also near the interfaces of GNPs/Cu (**Figure 2b**). The EDS analysis (inset, **Figure 2c**) reveals high concentrations of carbon and W elements and extremely low Cu content, suggesting that the GNPs are *in-situ* reacted with W particles during the SPS. This can also be confirmed from the XRD results (**Figure S5**). The selected area electron diffraction (SAED) pattern (**Figure 2c**) obtained from the marked region in

Figure 2b shows (012), (10-2) and (110) diffraction spots of W_2C along the [11-2] zone axis. The (10-10), (11-20) and (01-10) diffraction spots of GNPs along the [0002] zone axis are also observed (**Figure 2c**), revealing an orientation relationship between W_2C nanoparticle and GNPs, i.e. $[11\text{-}2]_{W2C}//[0002]_{GNPs}$. The *in-situ* formed tungsten carbides have caused significantly increased dislocation densities (**Figure S5**). Another representative TEM image in **Figure 2d** shows the unreacted W particles (confirmed by SAED shown in **Figure 2d**) are tightly attached to the Cu matrix and GNPs.

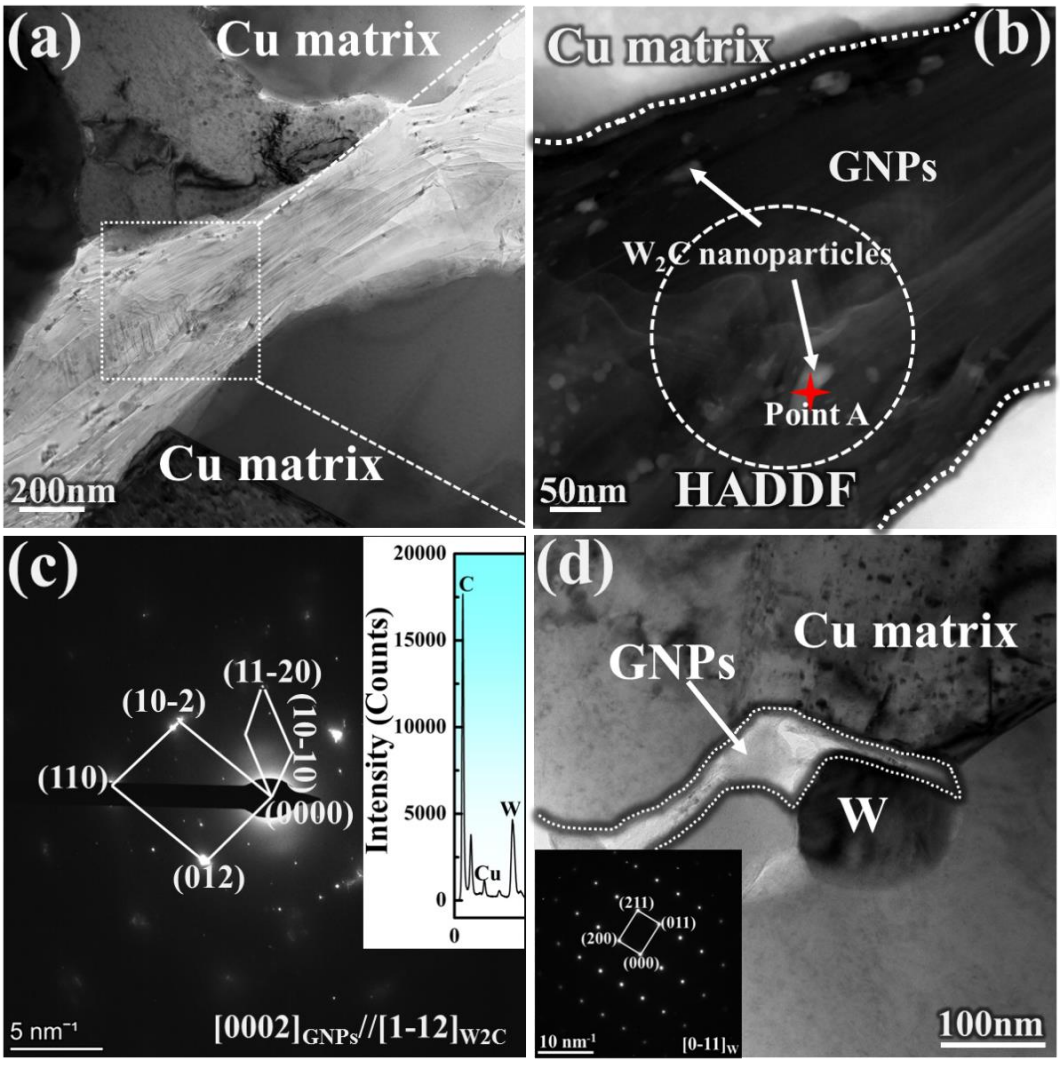

Figure 2. Typical TEM images taken at the interfaces of the GNPs-W/Cu composites

(a) TEM image, (b) High-angle annular dark-field- scanning transmission electron microscope (HADDF-STEM) image of the remarked region in Figure (a), (c) The SAED and EDS analysis of the marked region in Figure (b), (d) TEM image and SAED (inset) of black particle, respectively.

3.2 Raman and XPS Spectrum analysis

The structures of GNPs in the GNPs-W/Cu matrix composites before and after SPS were characterized using Raman spectroscopy and the results are shown in **Figure 3**. There are three characteristic peaks of the graphene [29], i.e. D band (~1340 cm^{-1}, the defect band), G band (~1580 cm^{-1}) and 2D band (~2700 cm^{-1}, also be called as G' peak), as shown in **Figure 3a**. The intensity ratio of the D band and G band can be used to evaluate the defects and quality of the carbon materials [30, 31]. However, in order to accurately estimate the GNPs' structure and defects in this work, we calculated the value of I_D/I_G by applying the Gaussian area numerical integration [22, 32] as shown in **Figure 3a.** The detailed parameters of Raman spectra of GNPs and GNPs-W/Cu composites are listed in **Table S1**. We can see that the ratios of I_D/I_G are slightly changed (with a variation of 0.06) for the GNPs-W/Cu mixtures compared with that of the original GNPs, which means that there are insignificant changes of the GNPs structures during the ball milling treatment. However, the I_D/I_G ratio for the GNPs-W/Cu composites is 0.70 which is much higher than that obtained from the mixed powders (0.24), revealing that the structure of GNPs is significantly changed, possibly due to the formation of carbides [33]. This can also be confirmed from the high resolution C 1s in X-ray photoelectron spectroscopy (XPS) spectra of GNPs in

GNPs-W/Cu composites shown in **Figure 3c**, in which the ratio of I_{sp2}/I_{sp3} is lower than that of original GNPs (**Figure S6**). As the intensity of sp^2 C=C is much higher than that of sp^3 C-C, this indicates that the GNPs have a high degree of graphitization and a low defect structure. Furthermore, **Figure 3c** shows a weak peak at the binding energy ~282.5 eV, which corresponds to that of the W-C bonds [34, 35], commonly observed in the SPS-processed GNPs-W/Cu composites. These results reveal that the sintering process causes the generation of a large quantity defects (including interfacial reaction product) and decreased content of sp^2 C domain.

The retention of GNP structure can be estimated by the characteristics of the Raman 2D peak. If the 2D peak is narrow and sharp, it might indicate that graphene has a single or low numbers of layer [36]. The 2D peaks will be split and broadened with the increase of number of graphene layers. Our results show that the multilayered GNPs exist in all the samples. The samples exhibit that the 2D peaks in **Figure 3b** are located at ~2717.68 cm^{-1} (raw GNPs), ~2708.07 cm^{-1} (GNPs-W/Cu powders) and 2682.66 cm^{-1} (GNPs-W/Cu composites), respectively. Obviously, the intensity of 2D peak becomes broadened and there is a negative shift of ~35.02 cm^{-1} after the SPS process, compared with those of the original GNPs, which is due to the increased contents of amorphous carbon [37, 38].

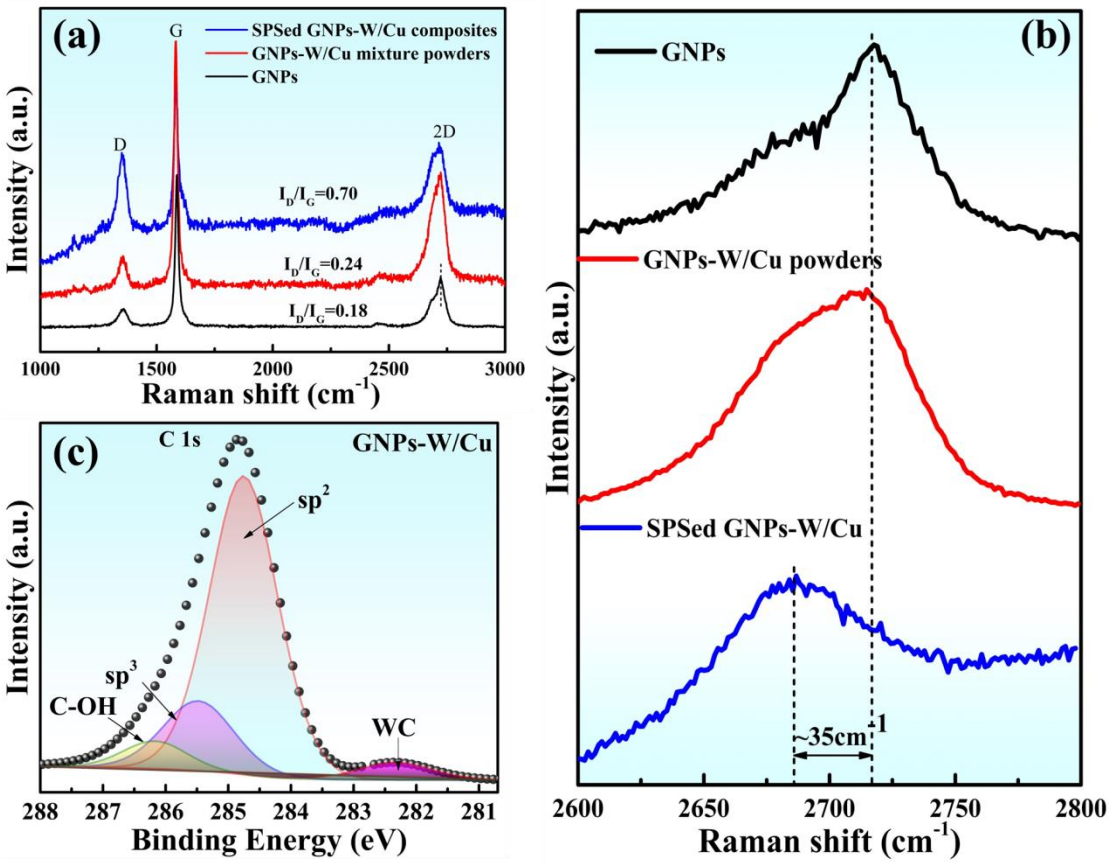

Figure 3. Raman spectra of (a) the GNPs-W/Cu composites before and after SPS processed, and (b) High magnification of the selected areas (2600~2800 cm^{-1}) of the Raman spectra curves in Figure (a). (c) High resolution C 1s XPS spectra of GNPs in GNPs-W/Cu composites, respectively.

3.3 Interfacial structures and characteristics

The interfacial structure and crystallographic orientation relationship in GNPs-W/Cu composites were further investigated using HRTEM images taken at different regions, and the representative analysis results are shown in **Figure 4**. Theoretically, there are six main types of interfaces in the composites, i.e. Cu-W, GNPs-Cu, GNPs-W, W_xC_y-GNPs, W_xC_y-Cu and W_xC_y-W. However, W and Cu have

no mutual solubility [39, 40] and their interfaces show simple physical bonding (**Figure S7**). Therefore, we focus on the other five types of interfacial microstructures. For the GNPs-Cu interfaces (**Figure 4a and a$_1$**), the FFT image shows the characteristic (002), (022) and (020) diffraction patterns of Cu. According to the noise-filtered IFFT image, the lattice inter-planar spacing was measured to be 0.182 nm, best matching the d-spacing of $(200)_{Cu}$. However, the corresponding IFFT (**Figure 4a$_1$**) image near the GNPs-Cu interface shows a high density of dislocations (blue ellipse) in GNPs owing to their deformation during the mechanical mixing and SPS [36]. Nevertheless, based on the measured inter-planar spacings from the IFFT image (**Figure 4a$_2$**), the misfit (ε) of $(0002)_{GNPs}$-$(110)_{W}$ is larger than 15%, revealing that the GNPs-W interface shows incoherently bonded structures. This type of interfacial structure may deteriorate the mechanical properties of the composite.

Regarding to the W_xC_y-GNPs interface shown in **Figures 4b~b$_6$**, the FFT diffraction patterns in **Figures 4b$_2$** and **b$_3$** show a specific orientation relationship of $(0002)_{GNPs}//(101)_{W2C}$ & $[-1210]_{GNPs}//[001]_{W2C}$. Based on the measured inter-planar spacings from the IFFT image (**Figure 4b$_1$**), the misfit (ε) of $(0002)_{GNPs}$-$(101)_{W2C}$ is 2.66%, revealing that the GNPs-W_2C interface is bonded coherently (**Figure 4b$_4$**). Indeed, a certain amount of W_2C-bonded GNPs are defective or amorphous, thus leading to the loss of graphene lattice periodicity and formation of a large distortion area (**Figures 4b$_5$~b$_6$**), which helps to improve the interfacial adhesion of GNPs-W_2C. In **Figure 4b**, the formation of carbides is due to the reactions between W and C elements (derived from GNPs) during the SPS. In fact, for the GNPs reinforced

MMCs, and also those composites with poor wettability (like Cu, Mg matrix composites), the *in-situ* formation of carbides at the interface is an easy and effective way to enhance the interfacial bonding of Cu and mechanical properties. For example, the excellent thermal conductivity of Cu matrix composites was achieved by using the *in-situ* formed Mo_2C coated diamond particles [41]. Recently, improved interfacial bonding and enhanced thermal/mechanical conductivity were achieved using TiC- or Mo_2C *in-situ* coated graphite fibers or graphene [42, 43].

Figure 4c shows the TEM image of the W_xC_y-Cu interface, in which a dense transition layer with a thickness of ~ 10 nm is observed between unreacted GNPs and Cu matrix, revealing that there is a good interface bonding of Cu matrix without the presence of visible interfacial voids or cracks. There are two kinds of GNPs at/near the W_xC_y-Cu interface, i.e. un-reacted GNPs (**Figure 4c$_1$**) and amorphous carbon region (**Figure 4c$_4$**). There are also other minor defects which have been introduced into GNPs, as observed in IFFT image of **Figure 4c$_1$**. Combining the FFT and IFFT results shown in **Figures 4c$_2$** and **4c$_3$**, the orientation relationship of $(-111)_{Cu}//(01-1)_{WC}$ & $[110]_{Cu}//[011]_{WC}$ can be obtained. The calculated misfit of $(01-1)_{WC}$-$(-111)_{Cu}$ interface is ~8.7%, revealing the formation of a semi-coherent interface, which is beneficial for the formation of strong interfacial bonding of Cu-WC interface. According the FFT/IFFT results shown in **Figure 4c$_4$**, there are amorphous structures of GNPs formed near the WC-Cu interface, which are mainly caused by ball milling mixed powder process (BMMP) [44]. Generally, various types of damage features (e.g., those newly generated surfaces, impurities, and crushed

structures, etc.) are produced during the BMMP, and they are attributed to the process of repeated deformation/crash, cold welding and fracturing.

Regarding to the W_xC_y-W interface shown in **Figure 4d**, a specific orientation relationship can be obtained, e.g., $(001)_{WC}//(110)_W$ & $[100]]_{WC}//[001]_W$. Based on the measured inter-planar spacings from the IFFT image, the corresponding misfits of $(001)_{WC}//(110)_W$ interface is ~10.7%, indicating the formation of a semi-coherent interface. Based on **Figure 4**, tungsten carbides of WC or W_2C in the form of nanoparticles or nanolayer are found in the interface of GNPs-W/Cu composites. The main reason is related to a kinetic-controlling mechanism, which has been discussed in details in Ref. [45]. Herein, both the formed interfacial WC nanoparticles and nanolayers act as "rivets" to tightly bind the GNPs inside the Cu matrix, leading to a strong interfacial bonding of GNPs/Cu composite. Especially some WC nanoparticles are embedded into the Cu matrix, resulting in a strong mechanical bonding between WC and Cu matrix. Furthermore, the improved wettability and bonding are established between GNPs and Cu phase by introducing WC transition layer or discontinuous W_2C nanoparticles, and the wettability of WC/Cu is better than that of Cu/C (i.e. GNPs) [46, 47]. Additionally, during the SPS process, W could be transferred from the carbides into the Cu matrix due to the slight WC dissolution, which could decrease the contact angle of WC/Cu [48].

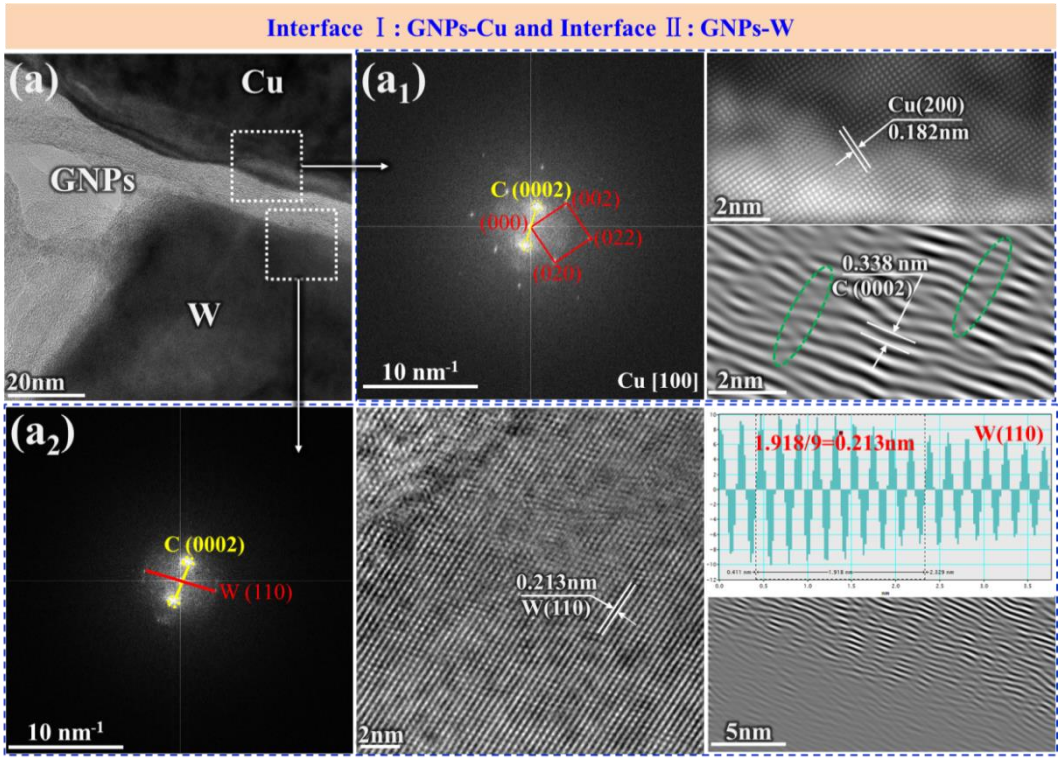
Interface Ⅰ: GNPs-Cu and Interface Ⅱ: GNPs-W
(a)
Cu
GNPs
W
20nm
(a1)
C (0002)
(002)
(000)
(022)
(020)
10 nm-1
Cu [100]
Cu(200)
0.182nm
2nm
0.338 nm
C (0002)
2nm
(a2)
C (0002)
W (110)
10 nm-1
0.213nm
W(110)
2nm
1.918/9=0.213nm
W(110)
5nm

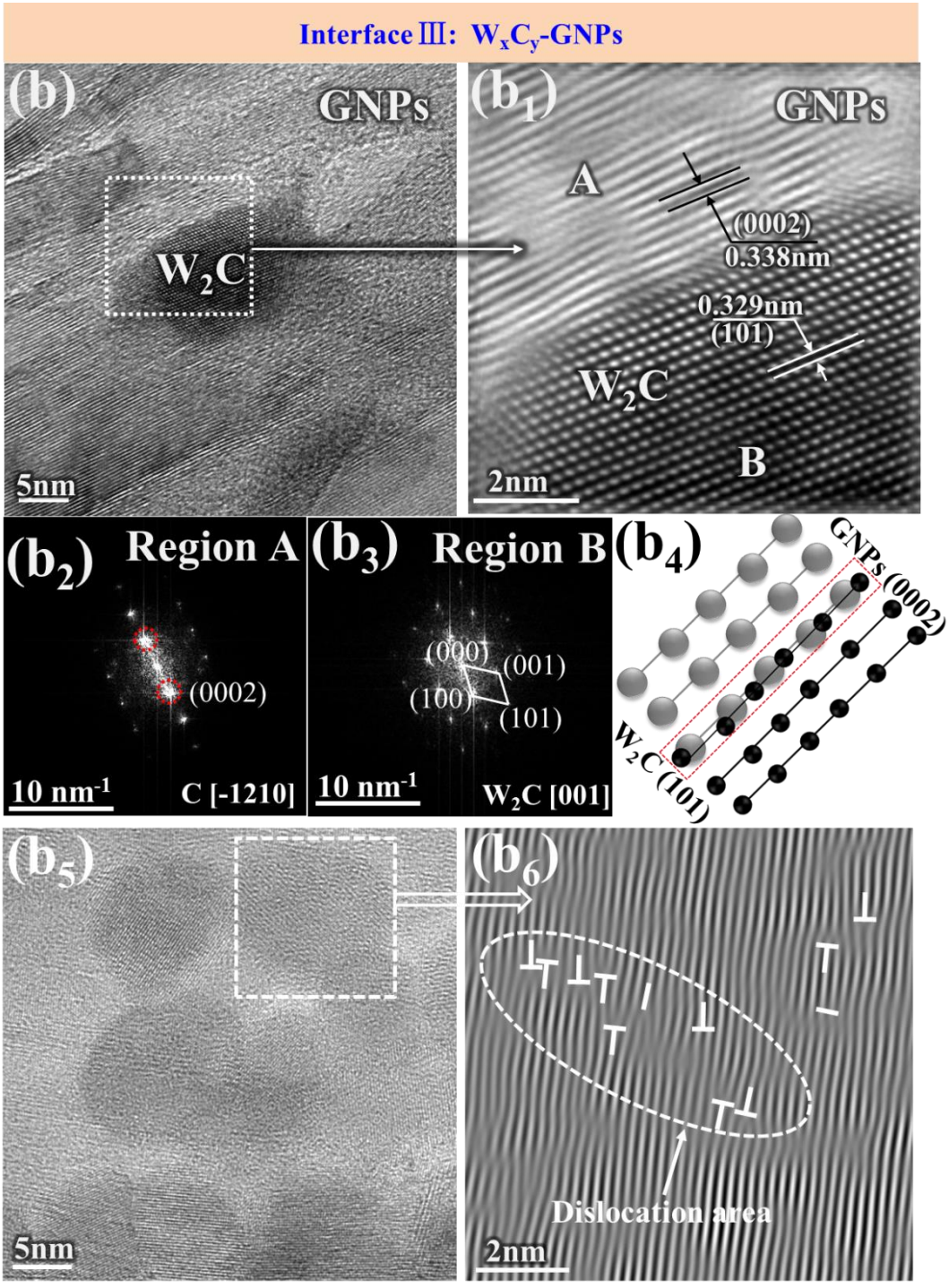
Interface Ⅲ: W_xC_y-GNPs
(b)
GNPs
W_2C
5nm
(b_1)
GNPs
A
(0002)
0.338nm
0.329nm
(101)
W_2C
B
2nm
(b_2)
Region A
(0002)
10 nm^{-1}
C [-1210]
(b_3)
Region B
(000)
(001)
(100)
(101)
10 nm^{-1}
W_2C [001]
(b_4)
GNPs (0002)
W_2C (101)
(b_5)
5nm
(b_6)
Dislocation area
2nm

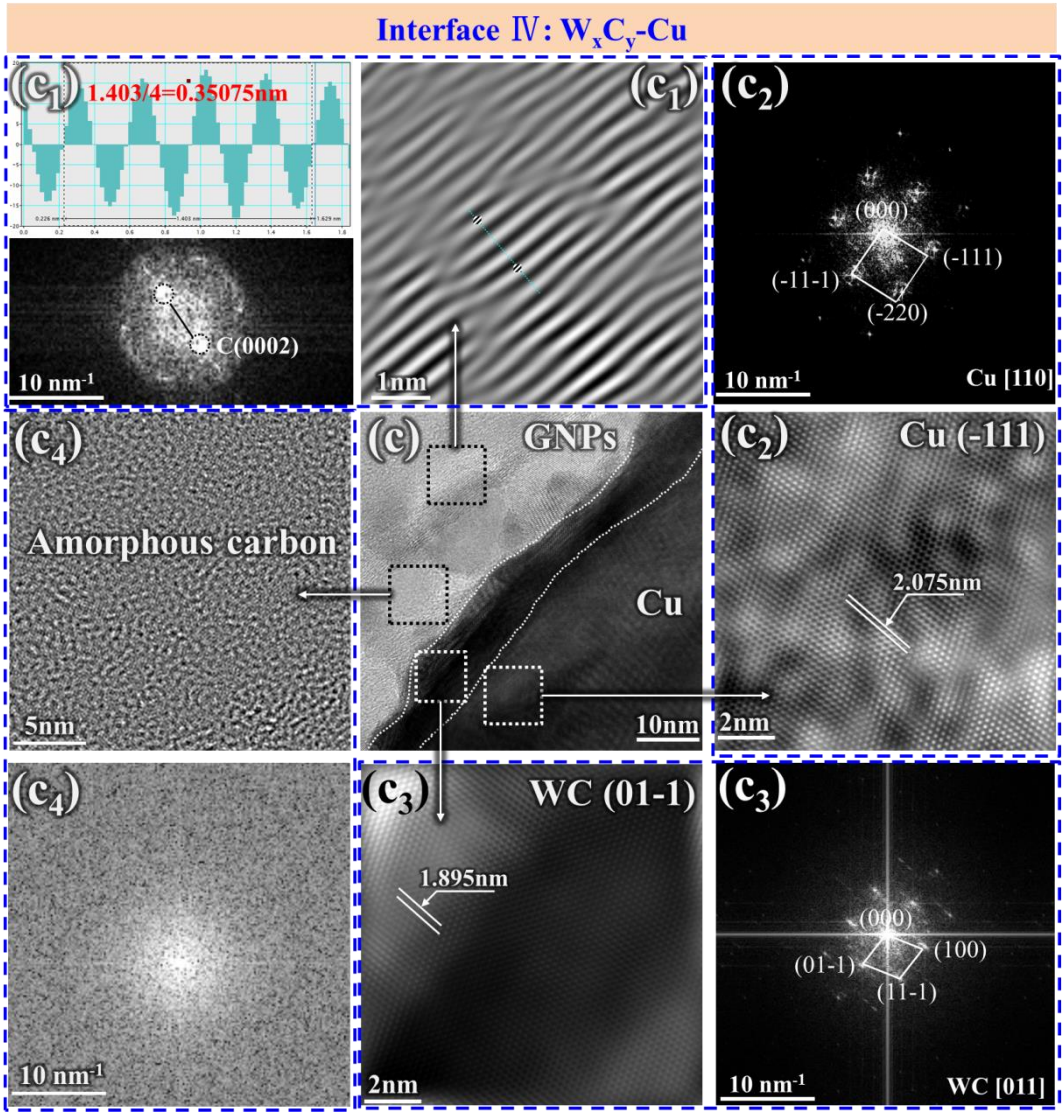
Interface Ⅳ: W_xC_y-Cu
(c1)
1.403/4=0.35075nm
C(0002)
10 nm-1
(c1)
1nm
(c2)
(000)
(-111)
(-11-1)
(-220)
10 nm-1
Cu [110]
(c4)
Amorphous carbon
5nm
(c)
GNPs
Cu
10nm
(c2)
Cu (-111)
2.075nm
2nm
(c4)
10 nm-1
(c3)
WC (01-1)
1.895nm
2nm
(c3)
(000)
(100)
(01-1)
(11-1)
10 nm-1
WC [011]

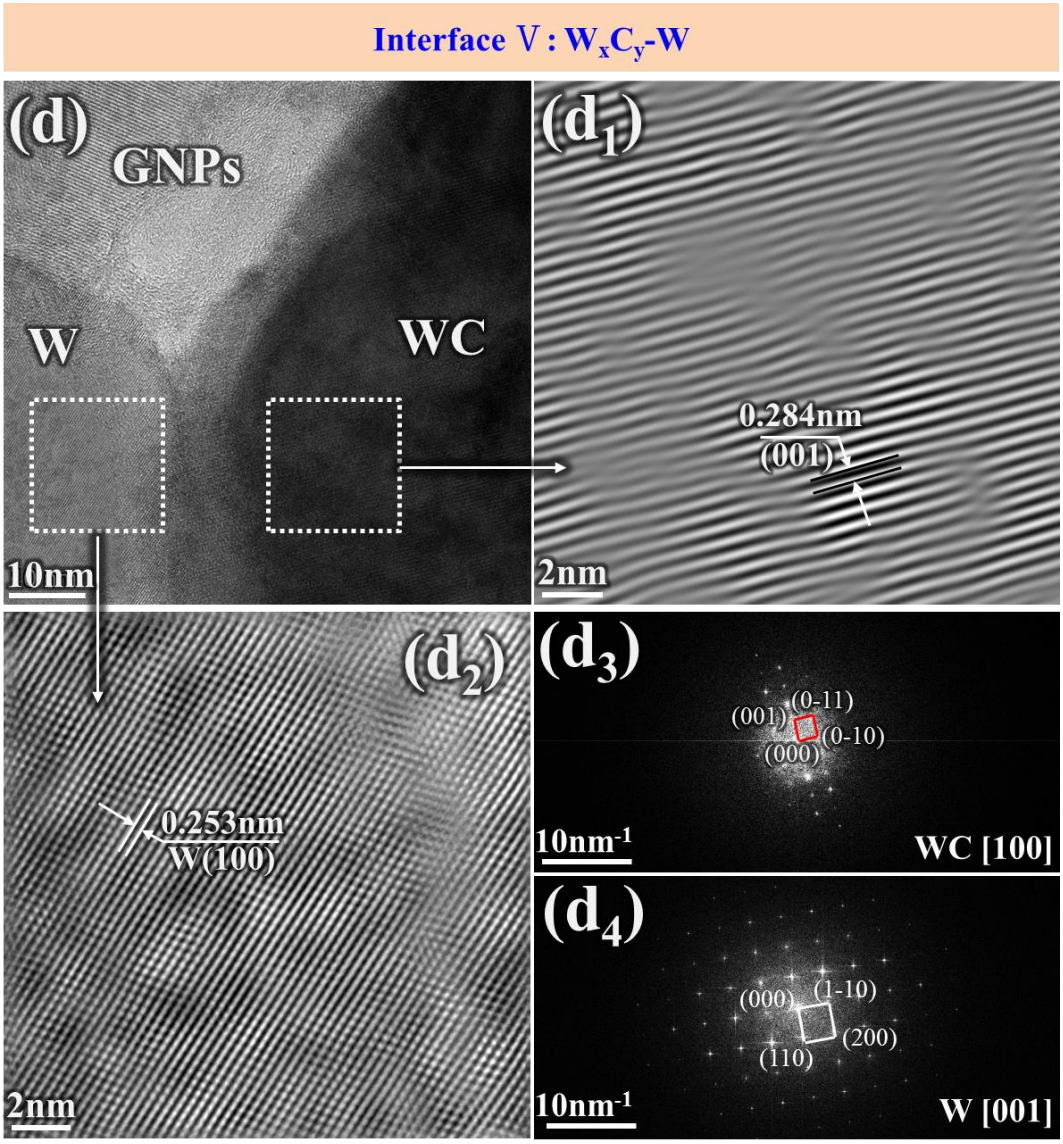

Figure 4. Detailed interfacial structures in GNPs-W/Cu composites. (a~a_2) Interface characteristic of GNPs-Cu and GNPs-W. (a) TEM image, (a_1) and (a_2) FFT, IFFT and corresponding lattice spacing measurement recorded at the marked regions in (a). (b~b_6) Interface characteristic of W_xC_y-GNPs: (b) HRTEM image, (b_1) IFFT recorded at the marked region in (b), (b_2) and (b_3) FFT diffraction patterns of region A and region B in (b_1), (b_4) A schematic illusion of the interface relationship between GNPs and W_xC_y nanoparticles, (b_5) HRTEM image of W_xC_y formed ar the defective GNPs, (b_6) IFFT recorded at the marked region in (b_5). (c~c_3) Interface characteristic of

W_xC_y-Cu: (c) TEM image, (c_1)~(c_3) FFT, IFFT and corresponding lattice spacing measurement recorded at the marked regions in (c). (d~d_2) Interface characteristic of W_xC_y-Cu: (d) TEM image, (d_1~d_2) IFFT and FFT diffraction patterns of marked region in Figure (d), respectively.

3.4 Physico-mechanical properties

Figure 5a shows the engineering stress-strain curves of the Cu matrix composites obtained from the tensile tests, and the obtained properties, i.e., the 0.2% offset yield strength (0.2% YS), ultimate tensile strength (UTS) and elongation at fracture are listed in **Table S2**. The 0.2% YS, UTS and elongation of the sintered pure Cu are 68.97±1.45 MPa, 103.50±2.28 MPa and 30.2±0.8%. These relatively poor strength compared with the composites are attributed to the weaker interfacial bonding between Cu and Cu grains after sintering [48]. Compared with those of the pure Cu, the GNPs/Cu and GNPs-W/Cu matrix composites exhibited remarkably enhanced strengths. The 0.2% YS and UTS values of GNPs/Cu sample are 110.16±1.80 MPa and 171.85±1.53 MPa, which are enhanced by about 59.42% and 66.02% compared with the sintered pure Cu matrix. It is interesting to see that the 0.2%YS and UTS of GNPs-W/Cu composites are 234.25±0.98 MPa and 295.65±1.12 MPa, which are enhanced by about 112.73% and 72.51% compared with GNPs/Cu samples. The elongation of GNPs-W/Cu composites is slightly increased from 10.8±0.3% to 13.5±0.9% in comparison with those of GNPs/Cu composites, which is attributed to a superior interfacial bonding strength. The elongations are higher that of

the Cu matrix reinforced with 1.0 vol. % fraction GNPs [49, 50]. The GNPs-W/Cu composites have achieved a good combination of high strength and good ductility.

The reinforcing efficiency (R) of graphene/metal composites can be defined as:

$$R = (\sigma_c - \sigma_m)/\sigma_m V_r \quad (3)$$

where σ_c and σ_m are the 0.2% YS of composite and the matrix, respectively, and V_r is volume fraction of reinforcements. The comparisons of values of R among CuMCs reinforced by graphene fabricated by four typical methods (including high-energy ball milling, molecular-level mixing, in-situ growth of graphene on Cu powders and using reduced graphene oxide metal coating) are plotted in **Figure 5b**. It can be found that our GNPs-W/Cu composite outperforms most graphene/Cu composites reported so far [32], suggesting the superior capacity of GNPs decorated with W_xC_y nanophase in reinforcing the Cu matrix. Certainly, the present processing ensures a strong interfacial bonding, which guarantees the exceptional strengthening ability of GNPs.

The measured hardness and physical properties of the SPS-processed samples are shown in **Figure 5c**. Compared with those of pure Cu samples, the hardness values of GNPs-W/Cu composites are increased from 45 HV to 58 HV, improved by ~28.9% owing to the higher relative density of the composites as well as synergetic strengthening of GNPs and W_xC_y. The improved densities of GNPs-W/Cu composites are attributed to: (1) the good wettability between GNPs and Cu due to the formation of W_xC_y; (2) the activated sintering of GNPs in the MMCs [43]; (3) the refined Cu grains owing to the effects of GNPs and W_xC_y on the grain growth during SPS.

The electrical conductivity (E_c) of the SPS processed pure Cu is 92 % IACS,

which is lower than that of 100 % IACS, and the main reason is that the electron transport channel is discontinuous due to the lower relative density. For GNPs-W/Cu composites, the E_c shows a slight reduction (~2.2%) compared with that of the pure Cu sample. The E_c of W_xC_y nanolayer formed in the composites is lower than that of Cu or GNPs, thus will hinder the electron transport and affect the conductivity. Apart from this, the orientation of GNP layer could also affect the conductivity. However, during milling, the orientation of the GNPs is difficult to control and is generally randomly distributed [61]. Previous studies report that the E_c of Cu was significantly decreased from 99.1% IACS (for Cu) to 51.6% IACS when 1.25 wt% GNPs was added, [49] and the reasons were attributed to the poor interfacial structure between Cu matrix and pristine graphene or reduced graphene oxide nanosheets. However, in this study, the conductivity has not been reduced significantly owing to the formation of good interfacial bonding. As shown in **Figure 5d**, a good balance between the electrical conductivity and strength can be well achieved. The superior mechanical and electrical properties, which are a vital requirement for many industry applications, can be attributed to the good interfacial bonding within the Cu matrix.

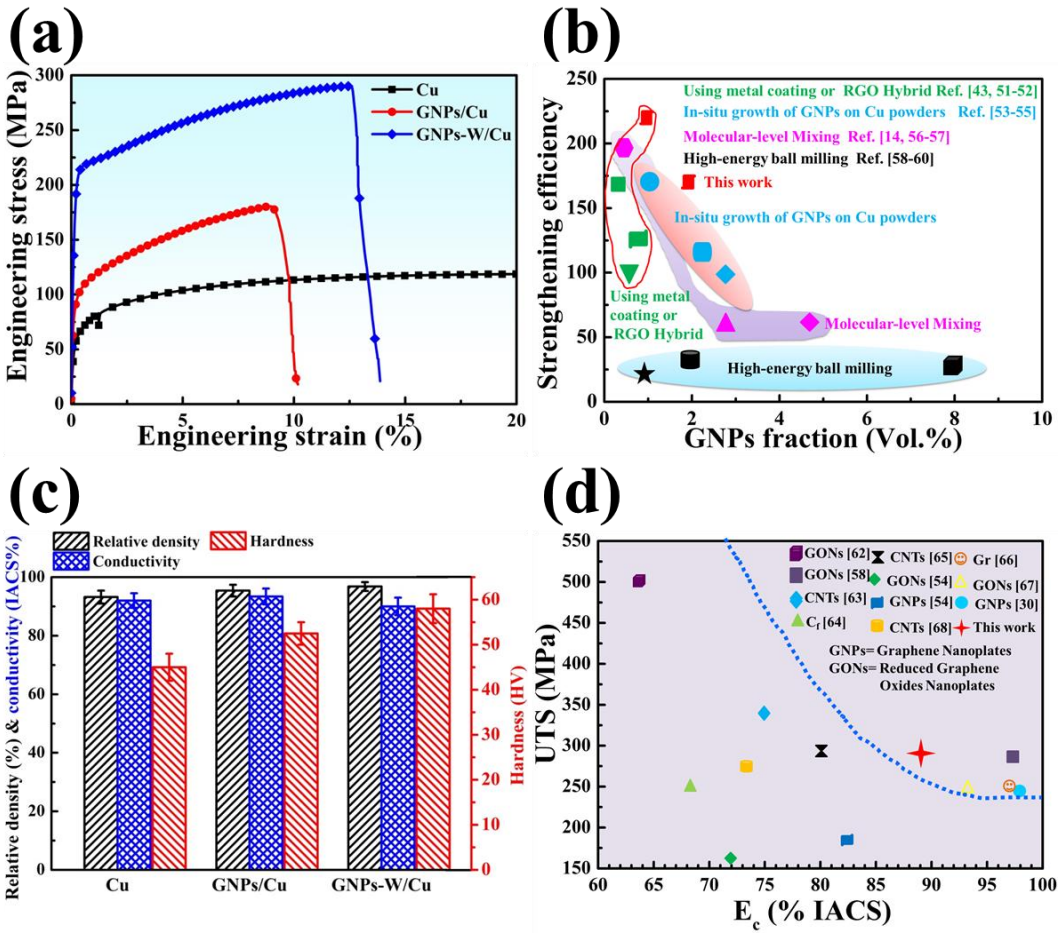

Figure 5. (a) Engineering stress-strain curves of the Cu matrix composites. (b) The reinforcing efficiency (R) of our graphene/Cu composites and those reported in literature prepared by four typical methods of high-energy ball milling, molecular-level mixing, in-situ growth of graphene on Cu powders and using reduced graphene oxide metal coating or hybrid [14, 43, 51-60], respectively. (c) Hardness, relative density and electrical conductivity of pure Cu and Cu matrix composites. (d) Ultimate tensile strength versus electrical conductivity (E_c, % IACS) of Cu matrix composites in comparison with other works [30, 49, 53, 62-68].

Figure 6 shows the typical SEM fracture morphologies of Cu matrix composites after the tensile test. It is obvious from **Figure 6a** that the fracture surface of pure Cu displays a typical ductile fracture with numerous dimples present over the entire

fractured surfaces. The fracture surfaces of GNPs/Cu (**Figure 6b**) and GNPs-W/Cu (**Figure 6c**) matrix composites still present some dimples, and some large and deep voids/cracks are observed around the fracture surfaces. These cracks were generated due to the large stress concentration and large differences in the coefficients of thermal expansion of GNPs [50] and Cu matrix during the tensile deformation. This will affect the ductility of composites, which can be verified by the results shown in **Figure 5a**. **Figures 6(c_1) and (c_2)** show that fractured surface of GNPs-W/Cu composites have both the bridged GNPs and fractured GNPs (as arrows denoted). The presence of bridged GNPs reveals that the well-bonded GNPs may prevent the fast crack propagation.

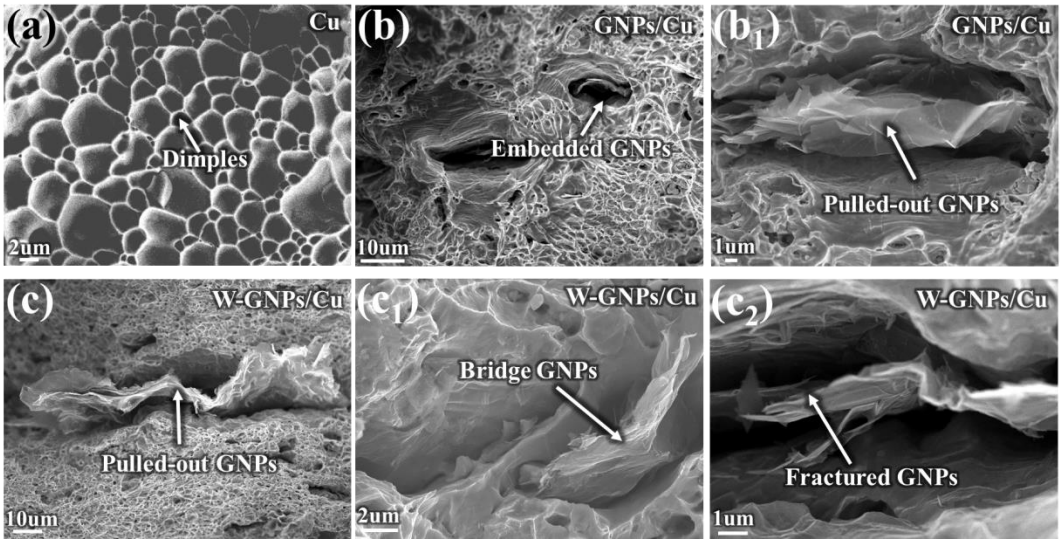

Figure 6. SEM fracture image of (a) Cu, (b~b_1) GNPs/Cu and (c~c_2) GNPs-W/Cu matrix composites after room temperature tensile test, respectively.

To further understand the role of GNPs for the improved mechanical properties of the GNPs-W/Cu composites, the *in-situ* microscale tensile tests were performed within the SEM in order to observe the real time fracture behavior of the GNPs in

GNPs-W/Cu composites. The results are shown in **Figure 7**. **Figure 7a** shows the photograph of the miniaturized tensile device for the tensile test. A notch was pre-made on the tensile sample to create the stress concentration site (**Figure 7b**), which is helpful for the localized crack initiation during the SEM observation. **Figure 7c** presents the tensile load-displacement curve marked with paused Stages ①~④ which are shown in **Figures 7d~g**, respectively. It is found in **Figure 7d** that a crack is initiated from the pre-made notch after a period of time after yielding (Stage ①). As the tensile displacement is increased, the initial crack propagates along a tortuous path coupled with the generation of new cracks ahead of the initial crack (Stage ②~③), thus ultimately leading to the composite fracture in Stage ④ (**Figure 7g**). The crack deflection mechanism helps to dissipate more energy and delay the catastrophic crack propagation, contributing to the extra-toughening and good ductility of GNPs-W/Cu composites [22, 69].

To disclose the GNPs failure mode, the magnified images of cracks are also obtained during the *in-situ* tensile test. The enlarged image in **Figure 7h** shows that the thin-layered GNPs with a length of ~ 15 um are tightly connected to the Cu matrix. **Figure 7i** shows that the pull-out GNPs are tightly embedded into the Cu matrix. Furthermore, some visible nanoparticles (denoted by white arrows) are covered on the surface of the pull-out GNPs (**Figure 7i**), which are believed to the W_xC_y nanoparticles observed in **Figure 2**. This reveals that these covered nanoparticles can effectively delay the GNPs' slippage upon tensile deformation, thus contributing to the efficient load transfer of GNPs-W/Cu composite.

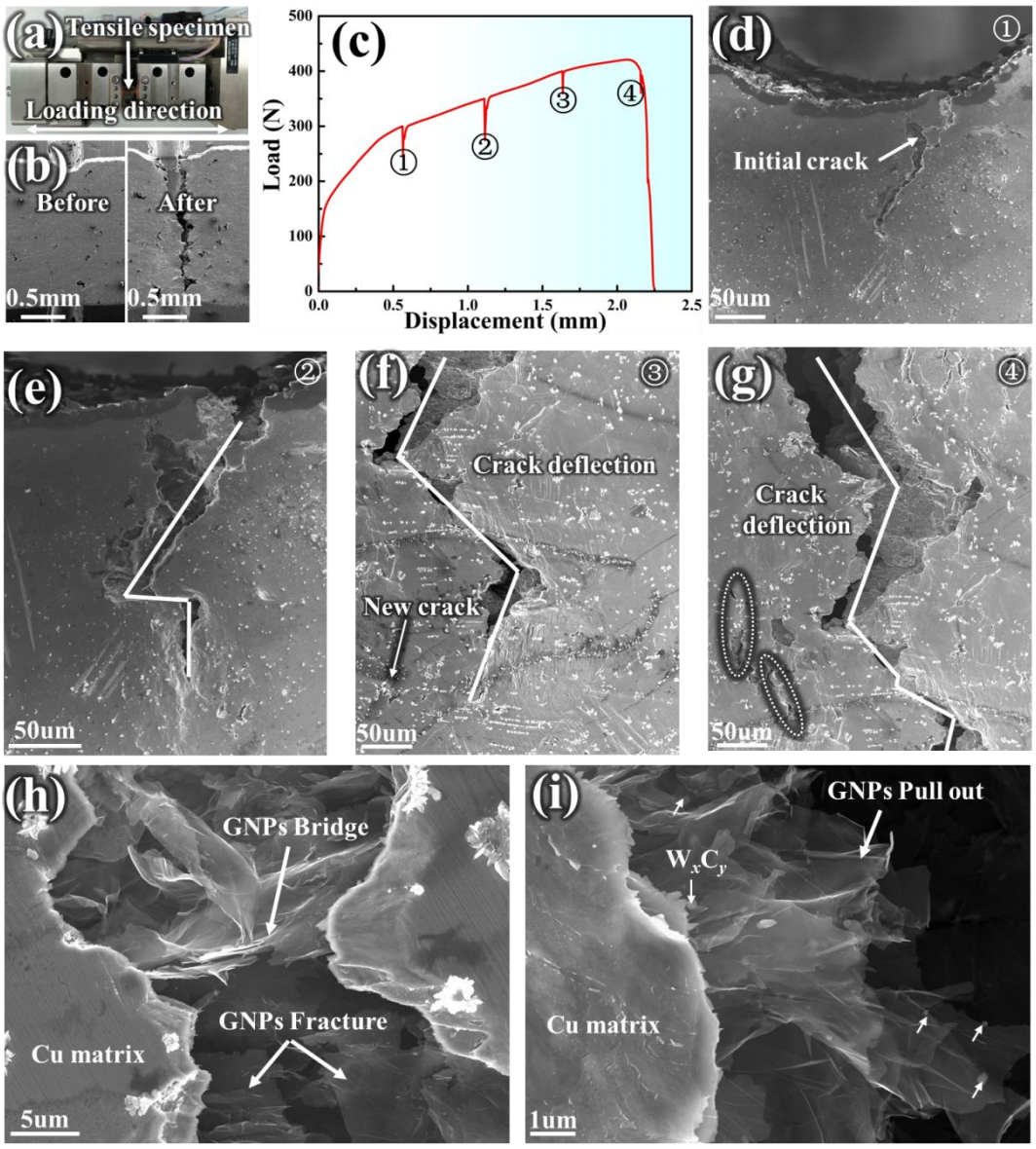

Figure 7. *In-situ* SEM observations of fracture behavior of GNPs-W/Cu composites during the tensile test. (a) Photograph of deformation device system installed in the SEM chamber. (b) SEM images of tensile sample before and after *in-situ* tensile test. (c) load–displacement curve of *in-situ* test with marked pauses. (d)~(g) SEM images of the crack evolution at the interrupted ①~④ Stages marked in (c). (h) ~ (i) Magnified images of the fractured surfaces, respectively.

3.5 Strengthening mechanism

Several mechanisms have been proposed to explain the strengthening effects of graphene in MMCs [67-73]: (1) Grain refinement in the MMCs via pinning effect; (2) Solution strengthening of the interstitial carbon, oxygen and nitrogen; (3) Dispersion strengthening of MMCs by the uniformly dispersed graphene; (4) Dislocation strengthening of in-situ formed carbides with the matrix, (5) Effective load transferring function from the matrix to graphene. However, the exact strengthening mechanisms for a given composite is dependent on the nature of its structures.

For the GNPs-W/Cu composites in this study, solution strengthening could be neglected because there is no solubility between carbon atoms in the Cu matrix [15]. For the thermal mismatch strengthening mechanism, the thermal mismatch between carbon and Cu are not significant after the composite is slowly cooled down to room temperature as in this study. Therefore, thermal mismatch mechanism might be only effective in those quenched composites, but it did not work well in the GNPs-W/Cu composites fabricated without any heat treatment.

Hence, we believe that the dominant strengthening mechanism of GNPs-W/Cu composites in present work are a combination of load transfer strengthening, dislocation strengthening and grain refinement, e.g.,

$$\sigma_c = \sigma_m + \Delta\sigma_d + \Delta\sigma_g + \Delta\sigma_{lt} \quad (4)$$

where σ_c and σ_m are the 0.2% YS of composite and matrix, and $\Delta\sigma_d$, $\Delta\sigma_g$, $\Delta\sigma_{lt}$ are the strengthening contributions from dislocation strengthening, grain refinement and load transfer strengthening.

(1) As shown in **Figure S5** and discussed in the supporting information, the

dislocation density of GNPs-W/Cu is significantly higher (~49.7%) than that of Cu without GNPs, revealing that enhanced interfacial bonding and *in-situ* formed W_xC_y interfacial products in the composite can effectively hinder the motion of dislocations. The improved 0.2% YS contributed by the dislocation strengthening in GNPs-W/Cu composites can be given using Eq. (5) [74]:

$$\Delta\sigma_d = \alpha G b(\sqrt{\rho_c} - \sqrt{\rho_m}) \quad (5)$$

where ρ_c and ρ_m are the dislocation density of composites and matrix, respectively, α is the geometric constant (1.25 [74]), G is the shear modulus of metal (42.1 GPa for Cu [75]), b is the magnitude of Burgers vector (0.256 nm [75]). Based on these data, the $\Delta\sigma_d$ is estimated as ~38.24 MPa.

(2) The GNPs and tungsten carbide particles are located around the grain boundaries, which will refine the Cu grains (**Figure S8**). This increased strength can be calculated using Hall-Petch relation [73]:

$$\Delta\sigma_g = k(d_c^{-0.5} - d_m^{-0.5}) \quad (6)$$

where d_c and d_m are the grain sizes of Cu matrix composites and pure Cu, respectively. k is the Hall-Petch coefficient of the Cu (140 MPa μm $^{1/2}$ [73]). Comparing the grain sizes shown in **Figure S8**, the grain size of Cu was effectively refined from ~135.7 μm to ~ 5.17 μm (GNPs-W/Cu). Based on Eq. (6), the obtained $\Delta\sigma_g$ is ~ 49.25 MPa.

(3) The improved 0.2% YS contribution originated from load transfer ($\Delta\sigma_{lt}$) can be acquired by subtracting the grain refinement effect ($^{\Delta}\sigma_g$) and dislocation strengthening ($^{\Delta}\sigma_d$). i.e. $\Delta\sigma_{lt}$ can be written as:

$$\Delta\sigma_{lt} = \sigma_c - \sigma_m - \Delta\sigma_d - \Delta\sigma_g \quad (7)$$

The obtained strengthening factors for the composites are summarized in **Table 1** and also shown in **Figure 8**. It is obvious from **Figure 8** that three main strengthening factors in GNPs-W/Cu composites are all synergistically enhanced. For example, the $\Delta\sigma_{lt}$ of the GNPs-W/Cu composites show a value which is 3.3 times higher than that of the GNPs/Cu composites, revealing that the superior load-bearing capability is due to the good interfacial bonding.

In general, according to the bonding types of reinforcements and metal matrix, their interfaces can be classified into: mechanical bond type, dissolve-infiltration type and reaction bonding type [76], in which the reaction bonding types of interface can significantly enhance the interfacial strength and effectively transfer stress or load during the tensile deformation. The SPS process applied in this work provides the good dynamic and thermodynamic conditions for the interfacial reactions. Thus, there are six major interfacial bonding regions existed in the Cu matrix composites (**Figure 4**). The GNPs-Cu interface is formed due to the non-solubility between Cu and carbon atoms, as a result, a weak interface bonding was produced between Cu and GNPs. The Cu-W interface is also only mechanical bond, however the un-reacted W particles make an important contribution to dislocations and refinement strengthening ($\Delta\sigma_d$ and $\Delta\sigma_g$). Some unreacted W particles are mechanically bonded with GNPs to form GNPs-W interface, which exhibits a little influence on the strength. However, three interfaces of W_xC_y-GNPs (**Figure 4b**), W_xC_y-Cu (**Figure 4c**) and W_xC_y-W (**Figure 4d**) are all the reaction bonding types. The good wettability and the enhanced interfacial

adhesion are improved in the GNPs/Cu matrix composites owing to the formation of W_xC_y, i.e. the *in-situ* formed W_xC_y nanoparticles on the surface of GNPs effectively restrain the dislocations' movement and enhance the transfer load capacity of GNPs ($\Delta\sigma_d$ and $\Delta\sigma_{lt}$). The transition nanolayer of dense W_xC_y between GNPs and Cu matrix can effectively transfer the loads and are strongly bonded with the copper particles, which significantly contributed to the values of $\Delta\sigma_{lt}$. The W_xC_y-W interfaces favor the enhanced interfacial adhesion of GNPs and unreacted W particles, which are beneficial to the $\Delta\sigma_{lt}$.

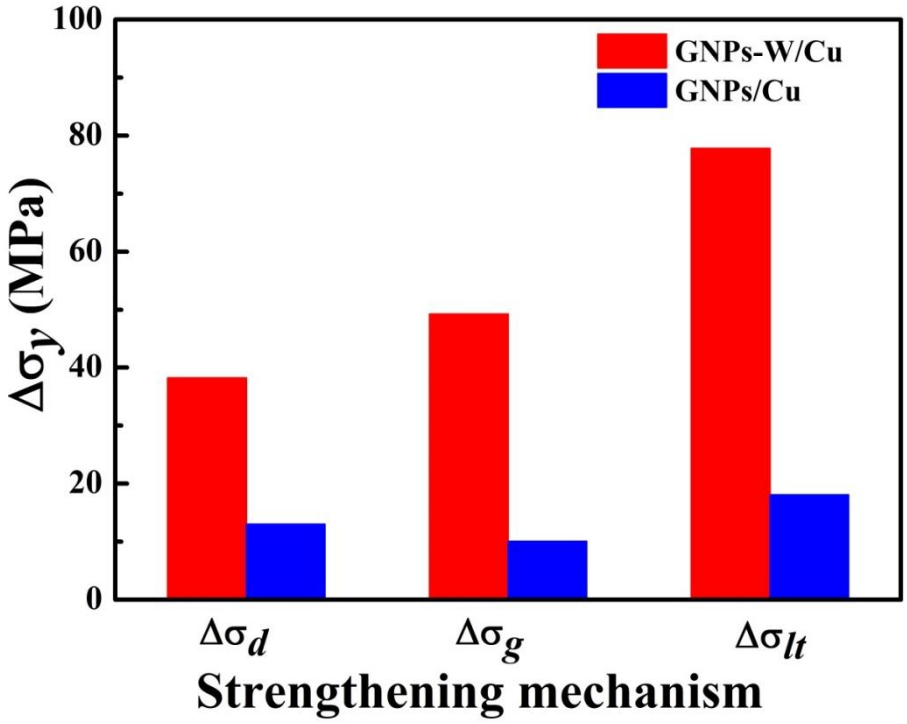

Figure 8. Comparisons of strengthening factors GNPs/Cu and GNPs-W/Cu matrix composites, respectively.

Table 1. Quantitative evaluation on the strengthening effect of grain refinement, dislocation strengthening and load transfer strengthening in Cu matrix composites.

Materials	$\triangle\sigma_d$ (MPa)	$\triangle\sigma_g$ (MPa)	$\triangle\sigma_{lt}$ (MPa)	$\triangle\sigma_y$ (MPa)	0.2% YS (MPa)
Cu	-	-	-	-	68.97
GNPs/Cu	13.03	10.07	18.09	41.19	110.16
GNPs-W/Cu	38.24	49.25	77.79	165.28	234.25

* $\triangle\sigma_y=\triangle\sigma_d+\triangle\sigma_g\triangle+\sigma_{lt}$

Based on the above discussions, the carbide formation shows a significant effect on the mechanical properties and interfacial structure of the Cu matrix composites. The formation of W_xC_y nanophases can be tailored using sintering of W-GNPs/Cu mixtures at various temperatures (700 °C, 800 °C and 980 °C), keeping other sintering condition and GNPs, W contents the same as aforementioned composites. **Figure 9a** shows the Raman spectra of obtained composites sintered at different temperatures. In **Figure 9a**, the value of I_D/I_G is increased from 0.48 to 0.86 when the sintered temperature is increased from 700 °C to 980 °C, revealing more interfacial products are produced (**Figures 9c~e**). It is worth noting that in **Figure 9b** the strength of GNPs-W/Cu composites sintered at 980 °C is lower than that sintered at 900 °C, suggesting that a thick W_xC_y interfacial layer on the GNPs-Cu interface can deteriorate the GNPs' structure and properties of final composites.

The present work provides a new strategy for strengthening Cu matrix (as well as other metal matrix) composites using the graphene via a low cost and easy powder metallurgy route. Furthermore, the local-alloying and interfacial engineering method

with *in-situ* carbide nanoparticles/nanolayers formation is considered to be superior to those of *ex-situ* carbide coating method (such as chemical vapour deposition, physical vaopur deposition, electroless plating, electroplating, etc.), because it is a simple and cost-effective approach, which can be readily scaled up for mass production.

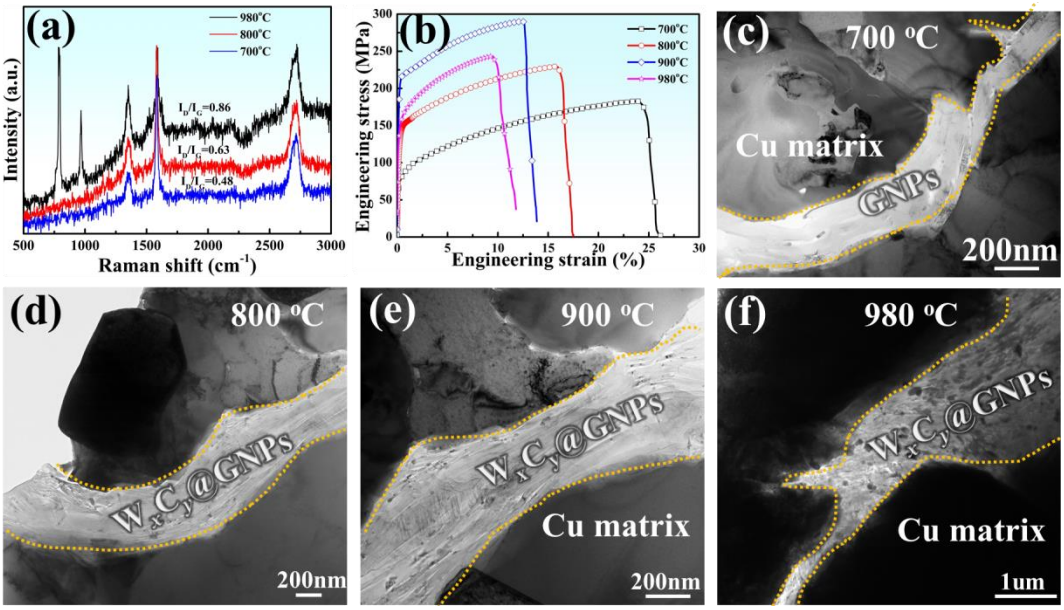

Figure 9. (a) Raman spectra and (b) Engineering tensile stress-strain curves, (c~e) Typical TEM image at the interface of GNPs-W/Cu composites sintered at 700 °C, 800 °C, 900 °C and 980 °C, respectively.

4. CONCLUSIONS

Combining interface engineering design and spark plasma sintering process, we have fabricated Cu matrix composites with high strength and excellent electrical conductivity using GNPs and *in-situ* formed W_xC_y nanophases as reinforcements. There are six major types of interfaces, i.e. GNPs-Cu, GNPs-W, Cu-W, W_xC_y-GNPs, W_xC_y-Cu and W_xC_y-W in GNPs-W/Cu composites. W_xC_y-GNPs, W_xC_y-Cu and W_xC_y-W are typical reaction bonding types, which are significantly contributed to the

dislocations strengthening and load transfer strengthening. GNPs-W and Cu-W interfaces make important contributions to dislocations and refinement strengthening. The GNPs-Cu interface exhibits a weak interface bonding, which shows a little improvement of strength. Compared with the SPS-processed Cu materials, the GNPs-W/Cu composites show much higher relative density, remarkably mechanical properties, e.g., their micro-hardness, 0.2% YS, and UTS have been enhanced by ~ 28.9%, 239.13% and 197.76%, with a high value of elongation. There is insignificant difference in the electrical conductivity after adding the GNPs and W_xC_y products. A strong interfacial bonding of Cu matrix composites is achieved by forming W_xC_y nano-layer and uniformly distributed carbide nanoparticles on the surface of GNPs and at/near the surface of Cu grains. The carbide nano-layer/particles play key roles with a bridging effect by linking the GNPs/Cu microstructures. Furthermore, the dislocation strengthening, refinement strengthening and load transfer strengthening were simultaneously achieved in GNPs-W/Cu matrix composites. The content of tungsten carbide can be controlled via tailoring sintering temperature. The present work provides a new strategy for the interfacial designs of carbon materials reinforced with Cu matrix composites with enhanced mechanical properties.

ASSOCIATED CONTENT

Supporting Information

Supporting Information is available from the Elsevier Publications or from the author.

Notes

The authors declare no competing financial interest.

ACKNOWLEDGMENT

The authors would like to acknowledge the financial support from National Natural Science Foundation of China (No. 51901192, 51777172), Key Research and Development Projects of Shaanxi Province (No. 2019GY-164, 2019GY-199, 2017ZDJC-19), Science and Technology Project of Weiyang District of Xi'an City (No. 201857), Shaanxi Youth Star Program of Science and Technology (No. 2020KJXX-061), as well as Newton Mobility Grant (No. IE161019) through Royal Society and the National Natural Science Foundation of China.

REFERENCES

[1] J. Hwang, T. Yoon, S.H. Jin, J. Lee, T.S. Kim, S.H. Hong, S. Jeon, Enhanced mechanical properties of graphene/copper nanocomposites using a molecular–level mixing process, Adv. Mater. 2013, 25, 6724–6729.
[2] M.A. Rafiee, J. Rafiee, Z. Wang, H. Song, Z.Z. Yu, N. Koratkar, Enhanced mechanical properties of nanocomposites at low graphene content, ACS Nano 2009, 3, 3884–3890.
[3] N. Khobragade, K. Sikdar, B. Kumar, S. Bera, D. Roy, Mechanical and electrical properties of copper-graphene nanocomposite fabricated by high pressure torsion, J. Alloy. Compd. 2019, 776, 123-132.
[4] K. Geim, K.S. Novoselov, The rise of graphene, Nat. Mater. 2007, 6, 183-191.
[5] S.C. Tjong, Recent progress in the development and properties of novel metal matrix nanocomposites reinforced with carbon nanotubes and graphene nanosheets, Mater. Sci. Eng. R 2013, 74, 281-350.
[6] C.G. Lee, X.D. Wei, J.W. Kysar, J. Hone, Measurement of the elastic properties and intrinsic strength of monolayer graphene, Science 2008, 321, 385-388.
[7] B.C. Fang, J.J. Li, N.Q. Zhao, C.S. Shi, L.Y. Ma, Boron doping effect on the interface interaction and mechanical properties of graphene reinforced copper matrix composite. Appl. Surf. Sci. 2017, 425, 811-822.
[8] X. Zhang, C.S. Shi, E.Z. Liu, N.Q. Zhao, C.N. He, Effect of interface structure on the mechanical properties of graphene nanosheets reinforced copper matrix

composites, ACS Appl. Mater. Inter. 2018, 10, 37586-37601.
[9] Z.R. Hu, G.Q. Tong, C. Zhang, H.F. Guo, J.L. Xu, C.J. Chen, Corrosion resistance and hardness of laser sintered graphene-copper nanocomposites, High Powder Laser and Particle Beams, 2015, 27, 1–6.
[10] G.S. Shao, P. Liu, K. Zhang, W. Li, X.H. Chen, F.C. Ma, Mechanical properties of graphene nanoplates reinforced copper matrix composites prepared by electrostatic self-assembly and spark plasma sintering, Mat. Sci. Eng. A 2019, 739, 329–334.
[11] C. Ayyappadas, A. Muthuchamy, A. Raja Annamalai, Dinesh K. Agrawal, An investigation on the effect of sintering mode on various properties of copper-graphene metal matrix composite, Adv. Powder Technol. 2017, 28, 1760–1768.
[12] B.H. Duan, Y. Zhou, D.Z. Wang, Y.R. Zhao, Effect of CNTs content on the microstructures and properties of CNTs/Cu composite by microwave sintering, J. Alloy. Compd. 2019, 771, 498–504.
[13] I.A. Ovidko, Metal graphene nano composites with enhanced mechanical properties: a review, Rev. Adv. Mater. Sci. 2014, 38, 190–200.
[14] F. Chen, J. Ying, Y. Wang, S. Du, Z. Liu, Q. Huang, Effects of graphene content on the microstructure and properties of copper matrix composites, Carbon 2016, 96, 836–842.
[15] B. Kong, T. Fan, J. Ru, Improved wetting and thermal properties of graphite-Cu composite by Cr-solution immersion method, Diam. Relat. Mater. 2016, 65, 191–197.
[16] Y.Z. He, F. Huang, H. Li, Y.W. Sui, F.X. Wei, Q.K. Meng, W.M. Yang, J.Q. Qi, Tensile mechanical properties of nano-layered copper/graphene composite, Physica E 2017, 87, 233–236.
[17] W.G. Chen, L.L. Dong, J.J. Wang, Y. Zuo, S.X. Ren, Y.Q. Fu, Synergistic enhancing effect for mechanical and electrical properties of tungsten copper composites using spark plasma infiltrating sintering of copper coated graphene, Sci. Rep. 2017, 7, 17836–17845.
[18] H. Wang, Z.H. Zhang, Z.Y. Hu, Q. Song, S.P. Yin, Z. Kang, S.L. Li, Improvement of interfacial interaction and mechanical properties in copper matrix composites reinforced with copper coated carbon nanotubes, Mat. Sci. Eng. A 2018, 715, 163–173.
[19] R.R. Jiang, X.F. Zhou, Z.P. Liu, Electroless Ni-plated graphene for tensile strength enhancement of copper, Mat. Sci. Eng. A 2018, 679, 323–328.
[20] X.N. Mu, H.N. Cai, H.M. Zhang, Q.B. Fan, F.C. Wang, Z.H. Zhang, Y.X. Ge, R. Shi, Y. Wu, Z. Wang, D.D. Wang, S. Chang, Uniform dispersion and interface analysis of nickel coated graphene nanoflakes/ pure titanium matrix composites, Carbon 2018, 137, 146-155.
[21] Y.Y. Jiang, Z.Q. Tan, G.L. Fan, Z.B. Zhang, D.B. Xiong, Q. Guo, Z.Q. Li, D. Zhang, Nucleation and growth mechanisms of interfacial carbide in graphene nanosheet/Al composites, Carbon, 2020, 161, 17-24.
[22] L.L. Dong, J.W. Lu, Y.Q. Fu, W.T. Huo, Y. Liu, D.D. Li, Y.S. Zhang, Carbonaceous nanomaterial reinforced Ti-6Al-4V matrix composites: Properties, interfacial structures and strengthening mechanisms, Carbon, 2020, 164, 272-286.
[23] J.W. Lu, L.L. Dong, Y. Liu, Y.Q. Fu, W. Zhang, Y. Du, Y.S. Zhang, Y.Q. Zhao,

Simultaneously enhancing the strength and ductility in titanium matrix composites via discontinuous network structure, Compos. Part A 2020, 136, 105971.
[24] K. Chu, F. Wang, X.H. Wang, Y.B. Li, Z.R. Geng, D.J. Huang, H. Zhang, Interface design of graphene/copper composites by matrix alloying with titanium, Mater. Des. 2018, 144, 290–303.
[25] K. Chu, J. Wang, Y.P. Liu, Z.R. Geng, Graphene defect engineering for optimizing the interface and mechanical properties of graphene/copper composites, Carbon 2018, 140, 112–123.
[26] R. Della Noce, S. Eugénio, K.I. Siwek, T.M. Silva, M.J. Carmezim, A.M.P. Sakita, R.L. Lavall, M.F. Montemor. Direct electrodeposition of hydrogenated reduced graphene oxide from unsonicated solution and its electrochemical response, Diamond & Related Materials 104 (2020) 107740
[27] J.H. Zhu, S.L. Feng, F.Y. Chu, X.Q. Feng, G.X. Xie, L.T. Yan, L. Li, Development of ceramics standard samples used for X-ray fluorescence spectrometric analysis, Spectrosc. Spect. Anal. 2010, 30, 3143-3148.
[28] B. Chen, J. Shen, X. Ye, H. Imai, J. Umeda, M. Takahashi, K. Kondoh, Solid-state interfacial reaction and load transfer efficiency in carbon nanotubes (CNTs)-reinforced aluminum matrix composites, Carbon 2017, 114, 198-208.
[29] M.S. Dresselhaus, A. Jorio, M. Hofmann, G. Dresselhaus, R. Saito, Perspectives on carbon nanotubes and graphene raman spectroscopy, Nano Lett. 2010, 10, 751–758.
[30] M.S. Dresselhaus, G. Dresselhaus, P. C. Eklund, Science of fullerenes and carbon nanotubes, Carbon 1997, 35, 437–438.
[31] L. Liu, S. Ryu, M.R. Tomasik, E. Stolyarova, N. Jung, M.S. Hybertsen, M.L. Steigerwald, L.E. Brus, G.W. Flynn, Graphene oxidation: thickness-dependent etching and strong chemical doping, Nano Lett. 2008, 8, 1965–1970.
[32] L. L. Dong, W.G. Chen, N. Deng, C.H. Zheng, A novel fabrication of graphene by chemical reaction with a green reductant, Chem. Eng. J. 2016, 306, 754–762.
[33] K. Chu, C.C. Jia, L.K. Jiang, W.S. Li, Improvement of interface and mechanical properties in carbon nanotube reinforced Cu–Cr matrix composites, Mater. Des. 2013, 45, 407–411.
[34] K.A. Beadle, R. Gupta, A. Mathew, J.G. Chen, B.G. Willis, Chemical vapor deposition of phase-rich WC thin films on silicon and carbon substrates, Thin Solid Films 516 (2008) 3847–3854
[35] H. Lin, B.W. Tao, J. Xiong, Q. Li, Y.R. Li, Tungsten carbide (WC) nanopowders synthesized via novel core–shell structured precursors, Ceramics International 39 (2013) 2877–2881.
[36] A.C. Ferrari, J.C. Meyer, V. Scardaci, C. Casiraghi, M. Lazzeri, S. Piscanec, A.K. D. Jiang, K. S. Novoselov, S. Roth, A. K. Geim, Raman spectrum of graphene and graphene layers. Phys. Rev. Lett. 2006, 97, 187–401.
[37] A.C. Ferrari, Raman spectroscopy of graphene and graphite: Disorder, electron–phonon coupling, doping and nonadiabatic effects, Solid State Commun. 2007, 143, 47–57.
[38] J. Schwan, S. Ulrich, V. Batori, H. Ehrhardt, S.R.P. Silva, Raman spectroscopy

on amorphous carbon films, J. Appl. Phys. 1996, 80, 440–447.
[39] L.L. Dong, M. Ahangarkani, W.G. Chen, Y.S. Zhang, Recent progress in development of tungsten-copper composites: Fabrication, modification and applications, Int. J. Refract. Metal. Hard Mater. 2018, 75, 30–42.
[40] Y. Li, G.Q. Luo, Y. Sun, J. Zhang, Q. Shen, L.M. Zhang, Microstructure and mechanical properties investigation of W-Cu composites prepared from dual-layer coated powders, Appl. Surf. Sci. 2020, 516, 146098.
[41] R.X. Liu, G.Q. Luo, Y. Li, J. Zhang, Q. Shen, L.M. Zhang, Microstructure and thermal properties of diamond/copper composites with Mo_2C in-situ nano-coating, Surf. Coat. Tech. 2019, 360, 376-381.
[42] Q. Liu, X. He, S. Ren, T. Liu, Q. Kang, X. Qu, Effect of titanium carbide coating on the microstructure and thermal conductivity of short graphite fiber/copper composites, J. Mater. Sci. 2013, 48, 5810–5817.
[43] K. Chu, F. Wang, Y.B. Li, X.H. Wang, D.J. Huang, Z.R. Geng, Interface and mechanical/thermal properties of graphene/copper composite with Mo_2C nanoparticles grown on graphene, Compos. Part A 2018, 109, 267–279.
[44] S.J. Yoo, S.H. Han, W.J. Kim, A combination of ball milling and high-ratio differential speed rolling for synthesizing carbon nanotube/copper composites, Carbon 2013, 61, 487–500.
[45] Z.H. Xu, X. Zhang, N.Q. Zhao, C.N. He, Synergistic strengthening effect of in-situ synthesized WC_{1-x} nanoparticles and graphene nanosheets in copper matrix composites, Compos. Part A 2020, 133, 105891.
[46] L.M. Wang, M. Hu, Study on microstructure and properties of WC-Cu-Ni powder sintering layer, Powder Metall. Industry 2015, 25, 44–50.
[47] Y.R. Li, C. Hou, H. Lu, S.H. Liang, X.Y. Song, WC strengthened W–Cu nanocomposite powder synthesized by in-situ reactions, Int. J. Refract. Met. Hard Mater. 2019, 79, 154–157.
[48] J.L. Cabezas-villa, L. Olmos, H.J. Vergara-hernández, O. Jiménez, P. Garnica, D. Uard, M. Flores, Constrained sintering and wear properties of Cu−WC composite coatings, Trans. Nonferrous Met. Soc. China 2017, 27, 2214−2224.
[49] R.R. Jiang, X.F. Zhou, Q.L. Fang, Z.P. Liu, Copper–graphene bulk composites with homogeneous graphene dispersion and enhanced mechanical properties, Mater. Sci. Eng. A 2016, 654, 124–130.
[50] H.Y. Yue, L.H. Yao, X. Gao, S.L. Zhang, E.J. Guo, H. Zhang, X.Y. Lin, B. Wang, Effect of ball-milling and graphene contents on the mechanical properties and fracture mechanisms of graphene nanosheets reinforced copper matrix composites, J. Alloy. Compd. 2017, 691, 755-762.
[51] Y. Tang, X. Yang, R. Wang, M. Li, Enhancement of the mechanical properties of graphene–copper composites with graphene–nickel hybrids, Mat. Sci. Eng. A 2014, 599, 247–254.
[52] H. Luo, Y. Sui, J. Qi, Q. Meng, F. Wei, Y. He, Mechanical enhancement of copper matrix composites with homogeneously dispersed graphene modified by silver nanoparticles. J. Alloy. Compd. 2017, 729, 293–302.
[53] M. Cao, D.B. Xiong, Z.Q. Tan, G. Ji, A.A. Behnam, Q. Guo, Aligning graphene

in bulk copper: nacre-inspired nanolaminated architecture coupled with in-situ processing for enhanced mechanical properties and high electrical conductivity. Carbon 2017, 117, 65–74.
[54] X. Zhang, C.S. Shi, E.Z. Liu, F. He, L.Y. Ma, Q.Y. Li, J.J. Li, N.Q. Zhao, C.N. He, In-situ space-confined synthesis of well-dispersed three-dimensional graphene/carbon nanotube hybrid reinforced copper nanocomposites with balanced strength and ductility, Compos. Part A 2017, 103, 178–187.
[55] S.C. Tjong, Recent progress in the development and properties of novel metal matrix nanocomposites reinforced with carbon nanotubes and graphene nanosheets. Mater. Sci. Eng. R 2013, 74, 281–350.
[56] J.W. Hwang, T.S. Yoon, S.H. Jin, J.S. Lee, T.S. Kim, S.H. Hong, Enhanced mechanical properties of graphene/copper nanocomposites using a molecularlevel mixing process, Adv. Mater. 2013, 25, 6724–6729.
[57] B. Xiong, Y. Zhou, Y. Zhao, J. Wang, X. Chen, R. O'Hayre, The use of nitrogendoped graphene supporting Pt nanoparticles as a catalyst for methanol electrocatalytic oxidation, Carbon 2013, 52, 181–192.
[58] D. Zhang, Z. Zhan, Experimental investigation of interfaces in graphene materials/copper composites from a new perspective, RSC Adv. 2016, 6, 52219–52226.
[59] C. Zhao, J. Wang, Fabrication and tensile properties of graphene/copper composites prepared by electroless plating for structrual applications, Phys. Status. Solidi. A 2014, 211, 2878–2885.
[60] D. Miracle, Metal matrix composites–from science to technological significance, Compos. Sci. Technol. 2005, 65, 2526–2540.
[61] Q. Li, Y.F. Guo, W.W. Li, S.Q. Qiu, C. Zhu, X.F. Wei, M.L. Chen, C.J. Liu, S.T. Liao, Y.P. Gong, A.K. Mishra, L.W. Liu, Ultrahigh thermal conductivity of assembled aligned multilayer graphene/epoxy composite, Chem. Mater. 2014, 26, 4459-4465.
[62] R. Perez-Bustamante, D. Bolanos-Morales, J. Bonilla-Martinez, I. Estrada-Guel, R. Martinez-Sanchez, Microstructural and hardness behavior of graphene nanoplatelets/aluminum composites synthesized by mechanical alloying, J. Alloy. Compd. 2014, 615, S578-S582.
[63] W.M. Daoush, B.K. Lim, C.B. Mo, D.H. Nam, S.H. Hong, Electrical and mechanical properties of carbon nanotube reinforced copper nanocomposites fabricated by electroless deposition process, Mater. Sci. Eng. A 2009, 513-514, 247-253.
[64] L. Liu, Y. Tang, H. Zhao, J. Zhu, W. Hu, Fabrication and properties of short carbonfibers reinforced copper matrix composites, J. Mater. Sci. 2007, 43, 974-979.
[65] S. Zhao, Z. Zheng, Z.X. Huang, S.J. Dong, P. Luo, Z. Zhang, Y.W. Wang, Cu matrix composites reinforced with aligned carbon nanotubes: mechanical, electrical and thermal properties, Mater. Sci. Eng. A 2016, 675, 82-91.
[66] L. Wang, Z. Yang, Y. Cui, B. Wei, S. Xu, J. Sheng, M. Wang, Y. Zhu, W. Fei, Graphene-copper composite with micro-layered grains and ultrahigh strength, Sci. Rep. 2017, 7, 41896.

[67] D.B. Xiong, M. Cao, Q. Guo, Z. Tan, G. Fan, Z. Li, D. Zhang, Graphene-and-copper artificial nacre fabricated by a preform impregnation process: bioinspired strategy for strengthening-toughening of metal matrix composite, ACS Nano 2015, 9, 6934-6943.
[68] B. Chen, S.F. Li, H. Imai, J. Umedab, M. Takahashi, K. Kondoh, Inter-wall bridging induced peeling of multi-walled carbon nanotubes during tensile failure in aluminum matrix composites, Micron 2015, 69, 1–5.
[69] K. Chu, J. Wang, Y.P. Liu, Y.B. Li, C.C. Jia, H. Zhang, Creating defects on graphene basal-plane toward interface optimization of graphene/CuCr composites, Carbon 2019, 143, 85-96.
[70] K.S. Munir, Y.F. Zheng, D.L. Zhang, J.X. Lin, Y.C. Li, C. Wen, Microstructure and mechanical properties of carbon nanotubes reinforced titanium matrix composites fabricated via spark plasma sintering, Mat. Sci. Eng. A 2017, 688, 505–523.
[71] K. Vasanthakumar, N.S. Karthiselva, Niraj M. Chawake, Srinivasa Rao Bakshi, Formation of TiC_x during reactive spark plasma sintering of mechanically milled Ti/carbon nanotube mixtures, J. Alloy. Compd. 2017, 709, 829-841.
[73] F.M. Zhang, S.L. Liu, P.P. Zhao, T.F. Liu, J. Sun, Titanium/nanodiamond nanocomposites: Effect of nanodiamond on microstructure and mechanical properties of titanium, Mat. Des. 2017, 131, 144–155.
[74] R.J. Arsenault, N. Shi, Dislocation generation due to differences between the coefficients of thermal expansion, Mat. Sci. Eng. R 1986, 81, 175-187.
[75] W. Kim, T. Lee, S. Han, Multi-layer graphene/copper composites: preparation using high-ratio differential speed rolling, microstructure and mechanical properties, Carbon 2014, 69, 55-65.
[76] R. Pérez-Bustamante, C.D. Gómez-Esparza, I. Estrada-Guel, M. Miki-Yoshida, L. LiceaJiménez, S.A. Pérez-García, R. Martínez-Sànchez, Microstructural and mechanical characterization of Al–MWCNT composites produced by mechanical milling, Mat. Sci. Eng. A 2009, 502, 159–163.